Acc. Chem. Res. **1998,** *31,* 267−278

Fiber Optic Imaging Sensors

DAVID R. WALT*

The Max Tishler Laboratory for Organic Chemistry, Department of Chemistry, Tufts University, 62 Talbot Avenue, Medford, Massachusetts 02155

Received June 4, 1997

Introduction

Several trends have become apparent over the past decade in the area of chemical sensors. Foremost among these is a reduction in size, as ever-smaller sensors have been created with some sensors approaching the nanometer scale.[1−3] There are several compelling reasons why the trend toward smaller sensors is so attractive. First, small sensors allow small features to be measured, providing extremely high spatial resolution. Such high resolution provides us with the ability to measure chemical concentrations and gradients on scales smaller than an individual cell. A second aspect of smaller sensors is the reduced measurement volumes that can be accessed by such sensors. The ability to look at small volumes enables one to interrogate low absolute numbers of molecules while retaining relatively high concentrations. For example, in looking at the release of neurotransmitter from nerve cell vesicles, a small sensor can capture the relatively high local concentration of neurotransmitter released before it diffuses into the bulk medium.[4−6] In addition to being able to measure high local concentrations of analyte, such sensors have the ability to detect an incredibly low absolute number of molecules. For example, 1000 molecules confined to a femtoliter (10^{-15} L, 1 μm^3) is in the micromolar concentration range—a perfectly reasonable and relatively easy concentration to analyze. Obviously, smaller sensors enable the interrogation of even smaller absolute numbers of molecules without necessarily sacrificing sensitivity. In addition to size considerations, sensors must deal with different degrees of chemical complexity. Some solutions may be remarkably clean and contain only a single analyte of interest, while others may be complex mixtures in which the identities and concentrations of multiple species in the solution are unknown. The ability to measure multiple analytes simultaneously has driven the need to develop multi-analyte sensors which are oftentimes formatted as arrays. Such arrays can be either individual sensors bundled into an array format or sensor arrays created specifically for a multi-analyte format. A final trend that utilizes this array format is the creation of cross-reactive sensor arrays that obviate the need for designing sensors with absolute selectivity.[7,8] In such array sensors, the reactivity patterns generated upon exposure to an analyte or analyte mixture generate unique patterns that can be processed using pattern recognition software. Thus the burden for chemical selectivity is transferred from the sensor to signal processing.

All of these features—small size, small volume, multi-analyte capability, array format, and cross-reactivity—can be incorporated into optical sensor arrays. Optical sensors are information-rich; optical signals can be interrogated and collected at multiple wavelengths, with different signal intensities, different phases, polarizations, and excited-state lifetimes. In this account, I will describe the work conducted in my laboratory over the past decade in which we have employed optical imaging fibers to approach some of the many exciting capabilities of sensors described above.

Principles of Optical Sensing

Optical fibers are employed widely in the telecommunications industry for data and signal transmission. An optical fiber is comprised of two types of transparent media: the core, in which the optical signal is transmitted, and the clad, a thin layer of lower-refractive index material that surrounds the core. The refractive index mismatch enables the core-clad interface to act effectively as a mirror, enabling light introduced into the optical fiber to be transmitted, via total internal reflection, to the fiber's distal end. To create a sensor, an indicator is immobilized on the fiber's tip that changes its optical properties upon contact with the chemical species of interest—the analyte. In all the sensors prepared in our laboratory, we have employed fluorescent indicators for optical transduction. In this mode, excitation light is introduced into the proximal end of the fiber and travels via total internal reflection through the fiber to the distal end where it excites a fluorescent indicator immobilized on the fiber tip. Some of the isotropically-emitted fluorescence is recaptured by the fiber and carried back to a detection system which analyzes the returning signal. Changes in analyte concentration are manifested as changes in fluorescence intensity or emission wavelength, both of which can be analyzed by the detection system.

Optical Arrays

An optical imaging array is a coherent bundle of optical fibers, each possessing its own core and clad. During the fiber drawing process, the positions of the individual fibers (pixels) within the array are maintained. Such coherence enables images to be conducted from one end of the fiber to the other. During the drawing process all the fibers become fused, making such arrays easy to handle. Typical

David R. Walt was born in Detroit, MI, in 1953. He received a B.S. in chemistry from the University of Michigan, Ann Arbor, and a Ph.D. in organic chemistry and pharmacology from SUNY at Stony Brook in 1979. After postdoctoral studies at MIT, he joined the faculty at Tufts University in 1981 where he is now Robinson Professor of Chemistry. Dr. Walt served as department chairman from 1989 to 1996. His research interests include fiber optic sensors, fluorescent indicators, neurochemistry, and micro- and nanofabrication.

* Phone: (617) 627-3470. Fax: (617) 627-3443. E-mail: dwalt@emerald.tufts.edu.

S0001-4842(97)00069-1 CCC: $15.00
Published on Web 05/19/1998

arrays have 3000−100 000 individual pixels fused into a total diameter of 0.2−1.0 mm. Excitation light addresses all the pixels of the array simultaneously, and a two-dimensional detector, such as a CCD camera, detects the returning signals simultaneously. This architecture provides significant advantages for the sensing applications described below.[9]

Combined Imaging and Sensing

Optical imaging arrays can carry images from one end of the fiber to the other as a result of the coherent array architecture. We have utilized the imaging characteristics of the fiber to simultaneously image and measure local chemical concentrations with micron-scale resolution.[5] With most array based sensors, fabrication is nontrivial. In the case of optical arrays, fabrication of a high-density sensing array is straightforward; one simply spin coats the entire end of the optical array with a thin layer ($\leq 5\ \mu$m) of chemically-sensitive material. In the simplest demonstration of such a sensor, we have fabricated a pH-sensitive array by spin-coating an imaging fiber with a uniform, pH-sensitive polymer layer. Several steps are required to immobilize the polymer on the fiber surface.[4] First, the glass surface of the fiber is treated with γ-methacryloxypropyltrimethoxysilane which functionalizes the fiber surface with a methacrylate residue. Next, a solution of an acrylate monomer, a cross-linker, and acryloylfluorescein (a polymerizable form of the pH-sensitive dye fluorescein) is deposited on the fiber tip, and polymerization is initiated either by a thermal or photochemical polymerization process (eq 1). Monomers and unreacted

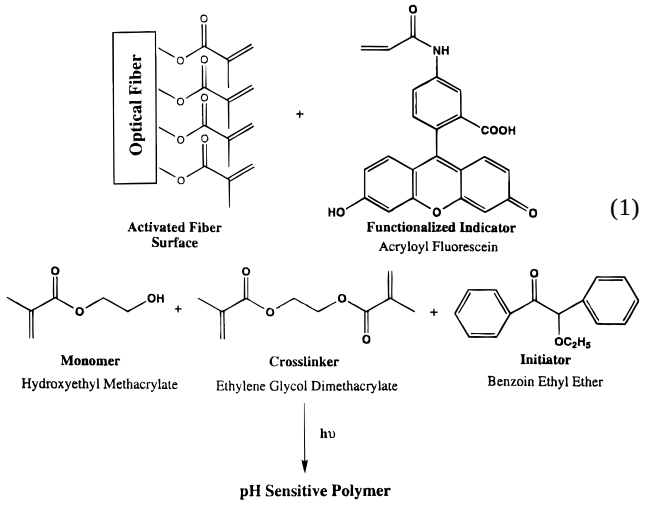

(1)

dye are then rinsed out of the polymer layer which is covalently bonded to the glass surface through the methacrylate groups of the attached silane. In this manner, an optical array sensor is created in which each pixel in the array imaging fiber is coated by a pH-sensitive polymer layer and acts as its own individual sensor. Imaging fibers with thousands of pixels have been coated with sensing layers providing thousands of individual microsensors spanning several hundred microns in diameter. We employed such a pH sensor microarray to

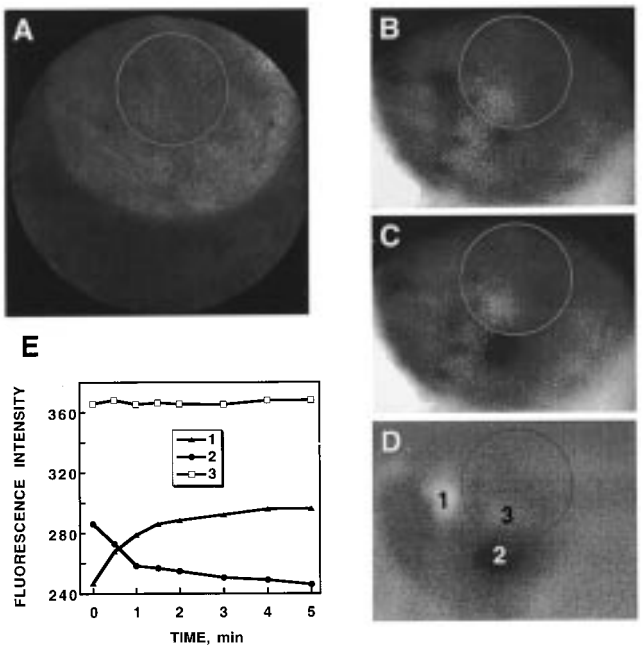

FIGURE 1. (A) White light image taken by an FITC/PAN-modified imaging fiber placed over an aluminum-cladded copper wire in a pH 6.0 phosphate buffer solution (0.1 M KCl). The circle in all figures denotes the Cu/Al border at the wire surface. Fluorescence images taken after (B) 2 s and (C) 5 min of exposure to the solution, (D) changes in the surface activity in the time period 2 s−5 min [region of interest corresponds to the wire surface area visible through the fiber (see white light image)]. High fluorescence intensities are denoted by white. (E) Average fluorescence intensities of the anodic sites (curves 1 and 2) and the cathodic site (curve 3) versus time. Lower fluorescence intensities correspond to lower pH values, higher intensities to higher pH values.

observe localized corrosion at metal surfaces.[10] The chemistry of corrosion initiation is of immense scientific as well as economic importance. Corrosion was monitored by employing a copper/aluminum galvanic pair. The reactions expected at the copper/aluminum interface under slightly acidic conditions are the reduction of water (eq 2) and/or reduction of oxygen (eq 3) at the cathodic sites, and dissolution of aluminum (eq 4) followed by ion solvolysis (eq 5) at the anodic sites. Cathodic reactions

$$2H_2O + 2e^- \rightleftharpoons 2OH^- + H_2 \qquad (2)$$

$$O_2 + 2H_2O + 4e^- \rightleftharpoons 4OH^- \qquad (3)$$

$$Al = Al^{3+} + 3e^- \qquad (4)$$

$$Al^{3+} + 3H_2O = Al(OH)_3 + 3H^+ \qquad (5)$$

produce hydroxide ion while anodic reactions generate protons. These processes can be investigated with the pH sensitive optical microarray by observing the pH-induced fluorescence changes occurring where the sensor contacts the metal surface. Under white light illumination, the fiber was positioned within several microns of the surface of the aluminum-coated copper wire.

As the fiber approaches the surface, one begins to see the image of the wire come into focus (Figure 1A). The

illumination light is then switched from the imaging mode (white light) to the fluorescence mode in which monochomatic light is introduced into the fiber. In the images shown (Figure 1), the brighter field corresponds to higher fluorescence intensity and a darker field to a lower fluorescence intensity, corresponding to high and low pH values, respectively. Within seconds, the array begins to distinguish different regions of the surface based on their local pH. By using image processing to subtract an early image from subsequent images, we were able to view dynamic features occurring over the metal surface as a function of time (Figure 1B−D). As can be seen in the images, regions are activated (Figure 1, spot 2, curve 2) and passivated (Figure 1, spot 1, curve 1) over the course of minutes, reflecting a rich chemistry taking place at the metal surface. By viewing such surfaces under different conditions, such as by varying the applied potential and adding inhibitors or inducers to the solution, we believe we can learn a tremendous amount about the nature and kinetics of the corrosion initiation process. After these images were taken, the sample was examined by scanning force microscopy and the structure of the metal surface was correlated directly with the active regions determined by the sensor array. We have been able to distinguish features as small as 6 μm using this sensing array technique.

A much more challenging application of these array sensors is the measurement of neurotransmitter release over relatively large surface areas. Wightman and coworkers have measured dopamine release from single cells.[11] Several groups have measured acetylcholine release useing acetylcholine biosensors.[12−16] For the most part, these efforts have been restricted to a single sensor or a few sensors, precluding spatial resolution of the sample being examined. We measured acetylcholine release from single dissociated cholinergic ciliary ganglion neurons from stage 34 white Leghorn chick embryos.[17−19] We first created an acetylcholine-sensitive indicating layer on the array surface, using chemistry similar to that described above for the pH sensor preparation.[4] In this sensor, the enzyme acetylcholinesterase was first immobilized into a polyacrylamide-*co*-*N*-acryloxysuccinimide (PAN)[4,20] polymer layer by allowing the enzyme's lysine residues to react with *N*-hydroxysuccinimide active esters during the diamine cross-linking reaction (eq 6).

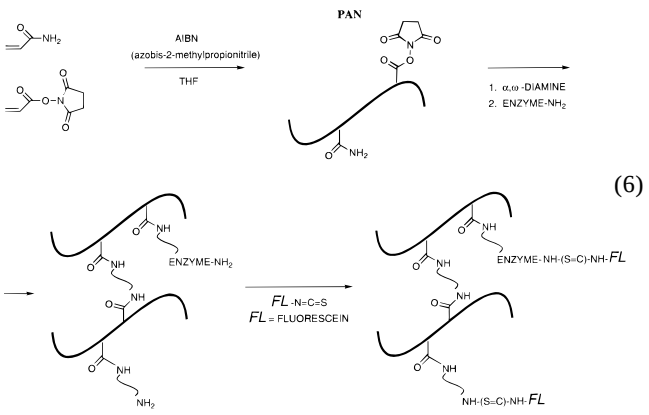

(6)

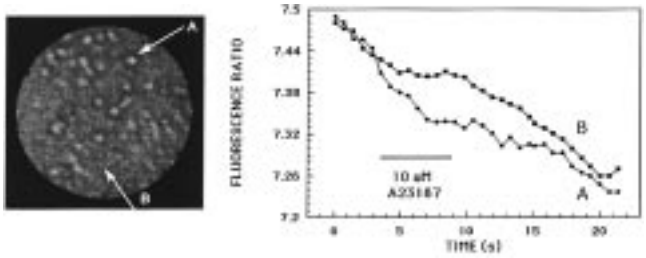

FIGURE 2. Preliminary biological measurements of an AChE-modified imaging fiber held in contact with dissociated ciliary ganglion neurons from white Leghorn chick embryos. (Left) White light image of dissociated ciliary ganglion neurons as viewed through the biosensor. In both the image and the graph. A is a region of the biosensor in contact with a ciliary ganglion neuron; B is a region of the biosensor not in contact with a ciliary ganglion neuron. The graph shows the biosensor's response upon stimulation with the calcium ionophore A23178. As seen in the graph, region A in contact with the neuron decreases its pH relative to control region B upon stimulation with the ionophore. Measurements were acquired with a 200-ms CCD acquisition time.

Residualamino groups in the resulting polymer were then allowed to react with fluorescein isothiocyanate (FITC) to create a polymer in which the fluorescein pH indicator was coimmobilized with acetylcholinesterase. As acetylcholine is released from cell surfaces it diffuses into the polymer layer where it is hydrolyzed to choline and acetic acid. Because the polymer acts as a diffusion layer, the product acetic acid acidifies the microenvironment of the polymer which can be measured as a fluorescence change by the pH indicator coimmobilized within the polymer layer. In contrast to the corrosion sensor discussed previously, the acetylcholine sensor employs ratiometric measurements. The pH dye fluorescein has different excitation spectra for the acid ($\lambda_{max} = 440$ nm) and base ($\lambda_{max} = 490$ nm) forms of the dye. Both forms have the same emission spectrum with a λ_{max} at 530 nm. By switching rapidly between the two excitation wavelengths, the ratio of the acid and base forms of the dye can be obtained. A given ratio is characteristic of a particular pH value and can be used to offset excitation source and detector sensitivity changes, dye leaching, and photobleaching effects.

The acetylcholine biosensor was positioned so that the sensing layer was in contact with the surface of the ciliary ganglion neurons. A capillary tube containing the calcium ionophore A23187 was placed at a 45° angle relative to the biosensor in order to evoke acetylcholine release using a pressurized pulse. Continuous ratiometric measurements were obtained by monitoring the fluorescence at 530 nm while switching between two excitation filters (490 and 440 nm). During chemical measurements, several frames were acquired before delivery of the secretion-inducing chemical to obtain background fluorescence intensity prior to the release of neurotransmitter. Once a sufficient number of background frames were acquired (e.g., 10 ratio pairs), acetylcholine release was evoked with a 3-psi pulse of calcium ionophore A23187. Figure 2 shows a greater decrease in fluorescence where the biosensor was in contact with a ciliary ganglion neuron

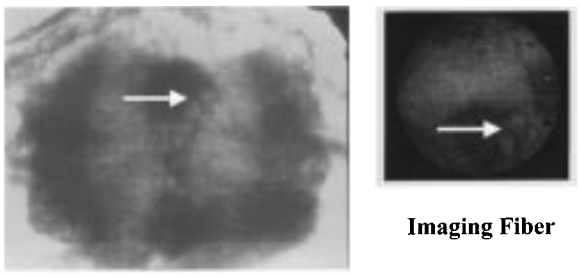

FIGURE 3. Dorsal cell bodies of an abdominal segment ganglion from the tobacco hornworm *Manduca sexta* as viewed through a microscope (left) and a 350-μm-diameter imaging fiber (right).

relative to the region of the biosensor not in contact with a neuron. The constant decrease in ratio is due to acidification of the medium resulting from basal metabolic activity. Controls in which buffer was delivered show no change in fluorescence.

The first biological demonstration of acetylcholine measurement in tissue was performed using a tobacco hornworm preparation.[21,22] The tobacco hornworm has sensory hairs on its prolegs which project to a neural ganglion known as a neuropil, Figure 3. It is known that acetylcholine is the neurotransmitter released upon sensory hair nerve stimulation. The acetylcholine sensor array was positioned over the neuropil. Once again, the white light image (Figure 3, right) shows clearly the morphological features of the neuropil. When the sensor was switched to the fluorescence mode and the neuropil was electrically stimulated, only the region expected to release acetylcholine changed its fluorescence intensity. The exciting aspect of this work is that neurotransmitter release could be observed over large areas of the tissue because of the high sensor density in the region surrounding the neuropil. Unfortunately, this biological specimen gave a rather uninteresting response pattern because of the release of acetylcholine from the relatively large structure being examined. We hope to use the sensor to observe much finer scale structures in tissues where cholinergic neurons are relatively well isolated from one another. The ultimate goal of such studies would be to study both the distribution as well as release patterns from complex neural tissue, perhaps providing neuroscientists with valuable information regarding connectivity of complex anatomical structures.

One of the limitations of the planar array approach is the relatively slow diffusion rate in the polymer layer which tends to cause a diffusional "bloom" leading to degradation of the spatial resolution. To address this problem, a modification of the sensor preparation protocol described above has led to sensor arrays with extremely fast-responding sensors.[23,24] A solution of monomer, cross-linker, functionalized indicator, and photoinitiator is placed on the distal tip of the fiber. Light is sent through the entire fiber array for a short period of time. Photoinitiation occurs only on the arrays' cores, resulting in a distinct chemical sensor on each fiber of

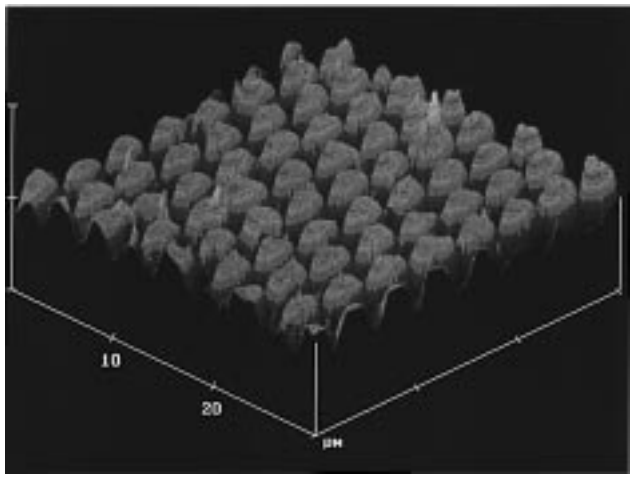

FIGURE 4. Atomic force microscope image of a polymer microstructure fabricated with (15−20%) (acryloxypropyl)methylsiloxane (80−85%) dimethylsiloxane oligomer. The individual polymer microspots have a diameter of 2.5 μm, as determined by the individual core diameters of the imaging fiber.

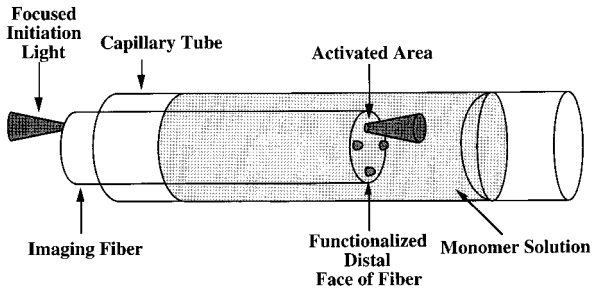

FIGURE 5. Setup of the photopolymerization procedure used to fabricate multicomponent fiberoptic chemical sensors.

the array, as shown in Figure 4. The hemispherical nature of these sensors enables radial diffusion to operate as opposed to planar diffusion, resulting in extremely fast-responding sensors. For example, oxygen sensors prepared this way have response times of 200 ms, while pH sensors have response times of 300 ms.[24] Such arrays should be useful for examining processes with subsecond kinetics. Chemical changes occurring over shorter time scales presently are limited by the acquisition and readout time of the CCD detector.

Multianalyte Arrays

A very different use of the optical imaging arrays is for multi-analyte sensing. In this approach, multiple sensors with different selectivities are placed in different spatial locations on the fiber's distal tip[25] shown in Figure 5. Light is focused onto the fiber's proximal end through a pinhole which enables illumination of a fraction of the array's pixels. Only the illuminated fibers convey light to the distal tip which is placed in a solution containing monomer, cross-linker, and the necessary indicators and/or biomolecules required to create a sensor. Once again, the entire distal surface of the optical fiber is prefunctionalized with a polymerizable silane. A shutter is employed to prevent illumination until the fiber is in place. When the shutter is opened, light exits a localized region of the fiber

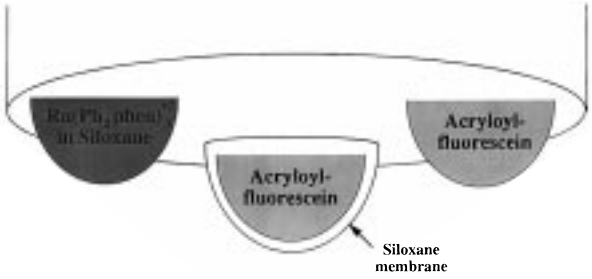

$$Ru(Ph_2phen)^{+2*} + O_2 \rightarrow Ru(Ph_2phen)^{+2} \qquad HInd \rightleftharpoons Ind + H^+$$

$$HInd \rightleftharpoons Ind + H^+$$
$$\updownarrow$$
$$CO_2 + H_2O \rightleftharpoons H_2CO_3 \rightleftharpoons H^+ + HCO_3^-$$

FIGURE 6. Chemistry associated with a multi-analyte sensor capable of measuring pH, CO_2, and O_2 simultaneously. The fluorescence of the ruthenium derivative, $Ru(Ph_2phen)_3^{2+}$, is quenched by oxygen. Fluorescein's fluorescence is strong in alkaline solutions. CO_2 penetration of the siloxane membrane generates acidic conditions behind the membrane.

and activates a photoinitiator contained in the polymerization solution. Because the light intensity is greatest close to the fiber surface, polymer forms exclusively and locally on the illuminated pixels. The bulk solution does not polymerize owing to the localized nature of light emanating from the fibers. Subsequent spots can be placed similarly on the fiber by moving the pinhole to different positions. To change the nature of the sensing material, the fiber is placed into different polymerization solutions containing different indicating chemistries. The final result is a sensor array on a unitary substrate containing multiple chemical sensing materials located in different spatial locations of the optical array. Thus, the sensors can be resolved spatially without requiring them to be separated spectrally. This approach enables the same indicator to be used for multiple sensors (e.g., enzyme-based biosensors).

In one example, such a multi-analyte array was used for simultaneously monitoring pH, CO_2, and O_2.[26] These three parameters are important in both bioprocess control and critical care monitoring. The ability to employ an optical sensor array with dimensions of several hundred microns provides a major advantage to monitoring bioprocesses because it involves a small displacement volume. For clinical applications, such a sensor may eventually be inserted directly into the bloodstream to provide continuous clinical measurements of these three parameters for critical care situations in which cardiovascular and respiratory function must be monitored. The chemistry comprising the three sensors is shown in Figure 6. The pH sensor is based on the immobilized fluorescein dye described above. The CO_2 sensor is based on the same pH dye contained within a polymer hydrogel, in this case, poly(hydroxyethyl methacrylate) cross-linked with ethylene glycol dimethacrylate. After placing two pH sensors on the optical fiber, the sensor is soaked in a bicarbonate buffer. The sensor is then dried and one of the pH sensing regions is overcoated with a hydrophobic silicone polymer. This polymer isolates the internal pH

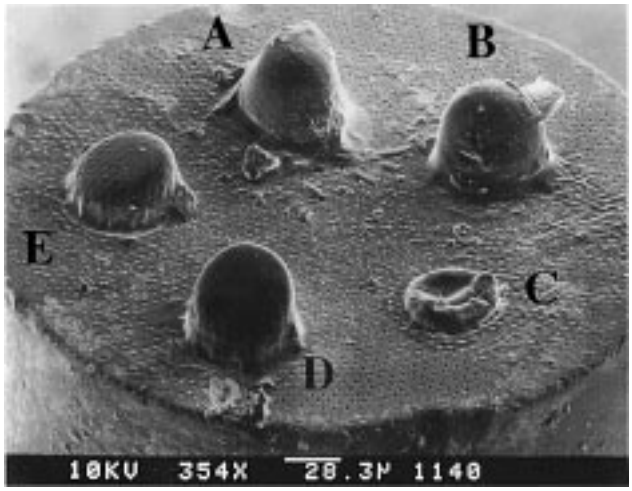

FIGURE 7. Scanning electron micrograph of a pH/CO_2/O_2 sensing array. The sensor was fabricated with two CO_2-sensitive matrices (A and B), one pH-sensitive matrix (C), and two O_2-sensitive matrices (D and E). The pH matrix collapsed due to the rapid evaporation of water because the sensor was subjected to a high vacuum during gold coating. In addition, the gas-permeable membrane of the CO_2-sensitive matrix (B) ruptured due to vacuum. Reprinted with permission from *Anal. Chim. Acta* (J. A. Ferguson, B. G. Healey, K. S. Bronk, S. M. Barnard, D. R. Walt. Simultaneous monitoring of pH, CO_2 and O_2 using an optical imaging fiber. Vol. 340, pp 123–131). Copyright 1997 Elsevier Science-NL, Sara Burgerhartstraat 25, 1055 KV Amsterdam, The Netherlands.

sensor from the external liquid medium but allows neutral gases to penetrate through the hydrophobic membrane. Therefore, the internal hydrogel can be rehydrated by soaking the sensor in water for several hours because water vapor penetrates through the silicone. CO_2 is also able to traverse the membrane. Upon contact of CO_2 with the hydrogel, H_2CO_3 is formed which dissociates into H^+ and HCO_3^-. This reaction causes the internal pH of the hydrogel to decrease which is detected and reported by the pH indicator. Thus, CO_2 is measured indirectly via its conversion into carbonic acid. This approach is similar to that used in the Severinghaus electrode, in which a pH electrode is covered by a gas-permeable hydrophobic membrane. The bulk pH of the medium does not affect the CO_2 sensor because the membrane is impermeable to ions. Finally, the O_2 sensor is prepared by incorporating a ruthenium indicator into a hydrophobic silicone membrane. Such ruthenium indicators are quenched by oxygen via collisional quenching.[27] A scanning electron micrograph of such a triple sensor is shown in Figure 7. We have employed such a sensor for monitoring a yeast fermentation as seen in Figure 8. The pH and CO_2 sensors were both monitored in the ratiometric mode as described above. The sensor is completely stable during the first 15 min of the fermentation. Upon addition of an inoculum of yeast, the pH decreases as a consequence of metabolic activity, O_2 decreases because residual O_2 in the medium is used by the yeast in an aerobic metabolic process, and CO_2 increases as a consequence of metabolism.[28] To our knowledge, this demonstration is the first simultaneous measurement of all three parameters using a single transduction mechanism in a unitary array format.

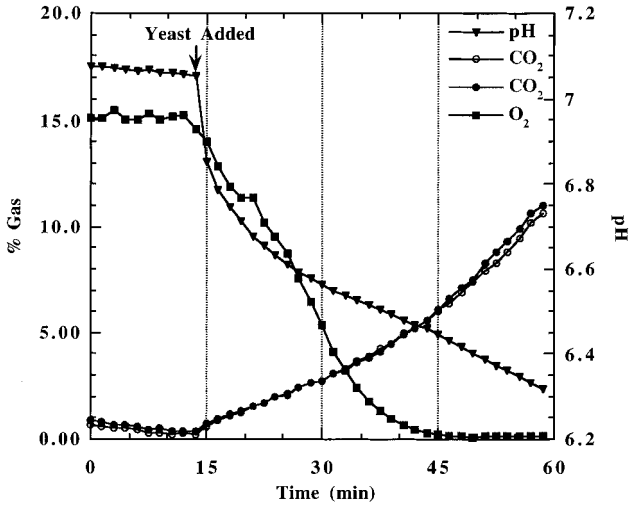

FIGURE 8. Concentrations of CO_2, O_2, and pH changing over the course of a beer fermentation. Changes occur only after the yeast was pitched. O_2 response was corrected for drift. The two CO_2 sensors in the array give identical readings. Reprinted with permission from *Anal. Chim. Acta* (J. A. Ferguson, B. G. Healey, K. S. Bronk, S. M. Barnard, D. R. Walt. Simultaneous monitoring of pH, CO_2 and O_2 using an optical imaging fiber. Vol. 340, pp 123−131). Copyright 1997 Elsevier Science-NL, Sara Burgerhartstraat 25, 1055 KV Amsterdam, The Netherlands.

Biosensors

Another area in which such multi-analyte sensors are valuable is in the area of biosensors. Biosensors couple a biological recognition element with a transducer. Common transducers include a pH or oxygen sensor. For example, an enzyme-based biosensor may operate by converting the analyte of interest (substrate) into a product. If either the substrate or product is acidic, the enzymatic reaction causes a local change in pH. Alternatively, O_2 utilizing or producing enzymes can be used to prepare biosensors if coupled to an O_2-sensitive transducer. The difficulty with such schemes is that the response of the sensor depends upon the pH or O_2 concentration in the sample as well as that of the analyte of interest. A change in the pH or O_2 of the sample solution will give an erroneous signal for analyte. We have integrated both the biosensing and transducing species into a single array format. A penicillin sensor was created using a pH-transducing biosensor by coimmobilizing both a pH indicator and the enzyme penicillinase within a single hydrogel.[29] Penicillinase catalyzes the hydrolysis of penicillin to penicilloic acid. Penicilloic acid dissociates into penicilloate and H^+. Because the hydrogel provides a diffusion barrier to H^+, the microenvironmental pH of the hydrogel is decreased relative to that of the bulk solution in the presence of penicillin. Thus penicillin is measured indirectly as a pH change and is reported by the immobilized fluorescent indicator. By placing two sensors on the optical array, one of which contains both the enzyme penicillinase and a pH indicator, and the other containing only the pH indicator, we can simultaneously monitor both the dependent and independent analytes. Thus, if the pH of the sample solution changes, both

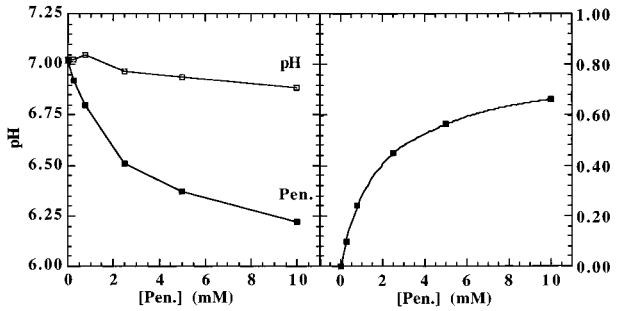

FIGURE 9. Response of a penicillin-sensitive (■) and a pH-sensitive (□) polymer matrix to increasing penicillin concentration (left). Plot of the difference between the buffer pH and the microenvironmental pH of a penicillin-sensitive matrix (ΔpH) versus penicillin concentration (right).

fluorescent indicators will be affected similarly; by measuring the difference between the two sensors we can monitor the penicillin concentration independent of the medium pH. This effect is shown in Figure 9 which shows that as penicillin concentration increases, the fluorescence signal decreases. The pH sensor on the same array remains relatively constant. When we carried out this type of experiment at a number of different pH's, we obtained a series of calibration curves showing the effect of the buffer pH on the resulting change in fluorescence as a function of penicillin concentration. The measured activity of the penicillin sensor depends on the activity of the penicillinase which in turn is affected by the pH of the medium in which the measurement is being made. Penicillinase has a maximum activity between 6 and 6.7. The calibration curves can be subjected to a kinetic analysis and fit to the Michaelis−Menten equation. The rearranged Michaelis−Menten equation shown below can then be used to generate a plot of K_m/pH vs pH.

$$[\text{Pen.}] = \frac{\Delta\text{pH}(K_m)_{app}/\Delta\text{pH}_{max}}{1 - \Delta\text{pH}/\Delta\text{pH}_{max}} \qquad (7)$$

By measuring the pH of the sample as well as the ΔpH between the pH and penicillin sensors, we can readily solve for the penicillin concentration. A glucose sensor based on the same principle was also prepared using the enzyme glucose oxidase in conjunction with an oxygen-sensitive indicator.[30] In the presence of glucose and glucose oxidase, oxygen is depleted which can be measured by the glucose biosensor. Comparison between the change in fluorescence of the biosensor and the oxygen concentration in the sample solution results in an oxygen independent measurement.

As more and more genes are identified as a result of the Human Genome Project there will be an increasing need to monitor gene expression both for diagnostic and genetic screening purposes.[31−34] We have utilized our optical imaging fibers to prepare genosensors capable of monitoring multiple gene sequences simultaneously.[35,36] To prepare such a genosensor, the copolymer of acrylamide and *N*-acryloxysuccinimide was photopolymerized in a discrete region on the sensor surface. This polymer contains active ester residues that react with amino

groups. An amine-terminated oligonucleotide was allowed to react with the active esters facilitating covalent attachment to the polymer surface. Residual active esters were then capped with ethanolamine. The procedure was repeated until the requisite number of oligonucleotide sequences was immobilized on the array surface. To test the ability of such an array to selectively bind to a target sequence, the array containing the immobilized oligonucleotides (the probes) was placed into a solution of fluorescein isothiocyanate-end-labeled oligonucleotide (the target) with a sequence complementary to one of the sequences in the array. In our initial experiments we designed a sensor using single core fibers that was capable of monitoring cytokine expression. Cytokines are immune-function regulators expressed to different degrees in immunohealthy and immunocompromised patients. As can be seen in Figure 10, selective hybridization occurred only when the complementary target sequence was present.[35]

To test the stringency of specificity for such an array, we evaluated the ability of the sensor to differentiate between two probe sequences with a single base-pair mismatch.[36] In this case we immobilized the H−Ras oncogene sequence as well as a single base-pair mismatch. In the presence of the H−Ras target, both probes hybridized at room temperature. As the temperature was raised, however, the single base-pair mismatch present on the mutant probe sequence lost fluorescence intensity as a result of dehybridization of the double strand. At 50 °C only the wild-type probe-target hybrid remained, demonstrating the ability of an optical sensor array to detect point mutations.[36] Furthermore, because of the extremely small size of the sensor, hybridization is rapid and the amount of sample required is minimal. In practice, DNA samples must be amplified using the polymerase chain reaction (PCR) to obtain sufficient quantities of DNA for analysis. By using smaller sensors the absolute amount of DNA required is reduced, in turn reducing the number of PCR cycles required.

Artificial Olfactory System

The conventional approach to creating sensors is to strive for absolute selectivity. In this approach, each analyte is measured by a specific sensor designed to be perfectly selective for that particular analyte. When achieved, this approach offers the ultimate in selectivity. An alternative paradigm is the one used by the mammalian olfactory system. The olfactory system contains millions of receptor cells each expressing one receptor type out of approximately 1000 different types of olfactory receptors.[37,38] Therefore, each receptor type is expressed by thousands of individual cells within the olfactory epithelium—the region where the receptor cells line the nasal cavity. From a number of neurophysiological experiments, it has been shown that upon exposure to any pure organic vapor approximately one-half of the olfactory cells respond.[39] The signals from these millions of cells are sent to the olfactory bulb which acts as a preprocessor, sending several thousand signals to the higher structures of the brain which then make the final identification of the odorous vapor. In this system, selectivity is not a function of an individual receptor type but is distributed among all the receptors in the array.[39] The burden is thus placed on processing the complex signal patterns, rather than attempting to design a receptor selective for each anticipated odor. This approach lends a tremendous amount of flexibility to the system and enables odors to be sensed that have never been encountered before. The key to the system is the information richness of the signals being sent to the processing system.

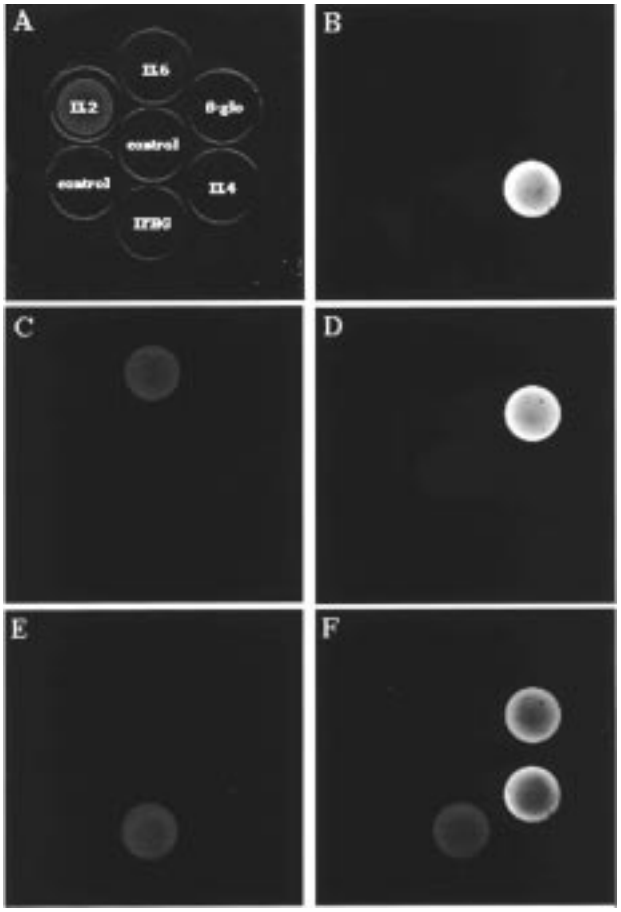

FIGURE 10. Fluorescent images of fiber optic biosensor array acquired in buffer solution after 5-min treatment with selected probe samples. High intensities are signified with white light: (A) after treatment with IL2 probe, (B) after treatment with IL4 probe, (C) after treatment with IL6 probe, (D) after treatment with β-glo probe, (E) after treatment with IFNG probe, (F) after treatment with a mixture of IL4, IFNG, and β-glo probes. Hybridized oligonucleotides were removed using a 90% formamide solution in Tris−EDTA buffer after each analysis. The signals obtained in buffer before hybridization were subtracted from the signals obtained after hybridization. Abbreviations: IL, interleukin; IFNG, interferon; β-glo, β- globulin. Reprint with permission from *Nat. Biotechnol.* (J. A. Ferguson, T. C. Boles, C. P. Adam, D. R. Walt. A fiber-optic DNA biosensor microarray for the analysis of gene expression. Vol. 14, pp 1681−84). Copyright 1996 Macmillan Magazines, Ltd.

We have attempted to mimic this system by creating an array of optical sensors containing a number of differentially cross-reactive sensing indicators.[7,8] The sensor array is based on the solvatochromic effect.[40,41]

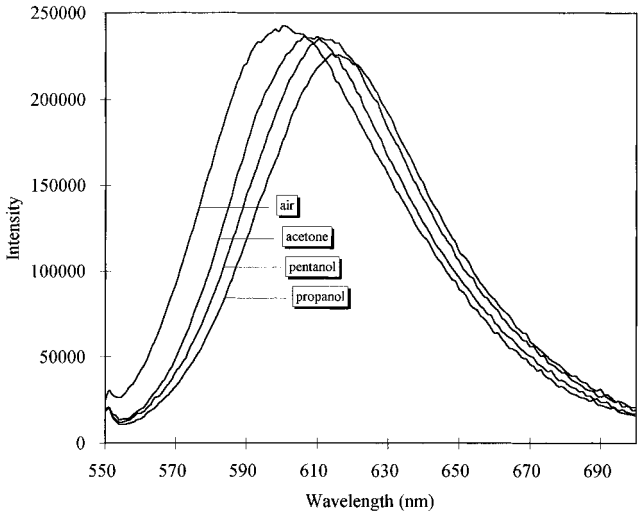

FIGURE 11. Emission spectra of a Nile Red/polycaprolactone sensor in environments of different polarity.

Table 1

PABS	poly(acrylonitrile−butadiene−styrene)
PSAN	poly(styrene−acrylonitrile) (75:25)
PSAA	poly(styrene−allyl alcohol)
PEG	poly(ethylene glycol)
DOW	poly(dimethyl siloxane)
PDPO	poly(diphenylene oxide)
PC	poly(caprolactone)
PBA	poly(1,4-butylene adipate)
PS802	(80−85%) dimethyl−(15−20%) (acryloxypropyl)-methylsiloxane copolymer
MMA	methyl methacrylate
RMS-044	4−6% (methacryloxypropyl)methylsiloxane, dimethylsiloxane copolymer
PS901.5	poly(acryloxypropyl)methylsiloxane)
PS851	(97−98%) dimethyl−(2−3%) (methacryloxypropyl)-methylsiloxane copolymer
CPS2067	(acryloxypropyl)methylcyclosiloxane
PS078.8	diethoxymethylsilyl-modified polybutadiene in toluene
PS078.5	triethoxysilyl-modified polybutadiene (50% in toluene)

Solvachromic dyes are affected by the polarity of the local environment. We have employed the dye Nile Red that changes both its absorption and emission spectra with polarity.[42] If Nile Red is dissolved in various solvents, the emission spectrum exhibits a bathochromic shift with increasing solvent polarity, Figure 11. We have employed this effect to create an array of differentially sensitive sensors. By immobilizing Nile Red into different polymer matrixes we create different baseline microenvironments for the dye. The polymers employed in this study are listed in Table 1. Some sensors were made by mixing two polymers. In a nonpolar polymer, Nile Red exhibits a relatively blue fluorescence emission spectrum, while in a polar polymer Nile Red exhibits a more red emission spectrum. Three effects are operative when the sensor array is exposed to an organic vapor. First, the different polymers partition vapors to different extents. In this way the local vapor concentration in each polymer is different. Second, depending on the polarity of the vapor relative to the polarity of the polymer, the fluorescence emission maximum will exhibit either a hypsochromic or bathochromic shift. Finally, the polymers swell to different extents as the organic vapor partitions into the sensing material. The result of these three effects is to create a

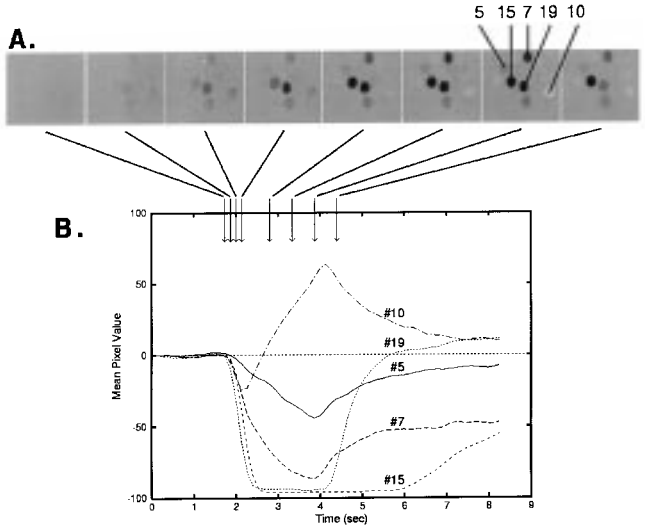

FIGURE 12. Examples of the data obtained from the fiberoptic array. Images in A illustrate raw data, showing changes in fluorescence of five fibers in the 19-fiber array in response to a 2-s pulse of saturated vapor benzene. The frames shown in A are taken at the indicated times in B. Graph B shows the quantitative responses of the five sensors as a function of time.

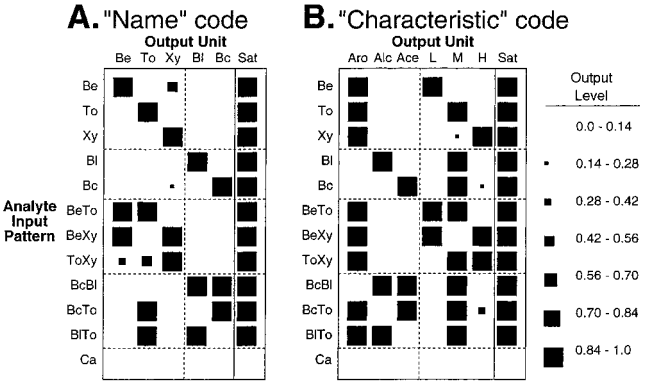

FIGURE 13. Input−output correlation diagrams showing the output of trained neural networks presented with test patterns of both single analytes and binary analyte mixtures. Analytes and mixtures were presented at saturated vapor. Results using the "name" output code are shown in A; results using the "characteristic" output code are shown in B. Abbreviations: BeTo = benzene + toluene; BeXy = benzene + xylene; ToXy = toluene + xylene; bcbl = butyl acetate + butyl alcohol; bcto = butyl acetate + toluene; BlTo = butyl alcohol + toluene. L, M, H, refer to low, medium, high molecular weights, respectively. Sat means saturated vapor.

complex response of the array upon exposure to a particular organic vapor (Figure 12).

Exposure of a vapor to the sensor array is not performed in a simple equilibrium manner. Animals present vapors to their olfactory receptors in a pulsatile manner, the result of sniffing. We have employed the same approach to generating sensor responses. A brief pulse of vapor is delivered to the optical fiber array resulting in a temporal response profile due to the three effects described above—partitioning, polarity, and swelling. The major contributors to the response profile are the compound's polarity and size. Polarity determines both the compound's partitioning into the various sensor/polymer matrixes as well as the resulting effect on the indicator's

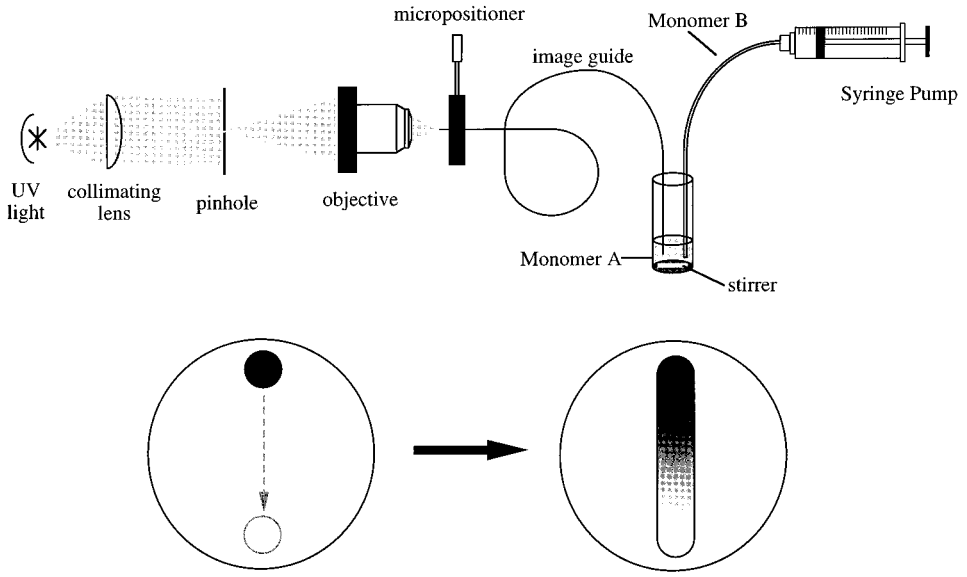

FIGURE 14. Schematic of gradient sensor fabrication apparatus and procedure.

emission properties. The molecule's size determines how rapidly it diffuses into the various polymer matrixes. Smaller molecules diffuse more rapidly than larger molecules. Each compound gives a relatively unique temporal response for each sensor in the array. With a large number of different sensors in the array, each organic vapor gives a complex response signature which can be used to train a pattern recognition system such as a neural network. Upon subsequent exposure of the sensor to the same vapor, the response pattern is readily recognized, enabling the array to identify the particular compound. In addition, networks can be trained to classify compounds into particular categories such as aromatic, alcohol, and ester, as well as to recognize the relative molecular weight of a particular compound. Finally, networks can be trained to recognize individual components of binary mixtures (Figure 13) suggesting that such a system will eventually be able to recognize components contained in complex mixtures. Ultimately the success of such an approach will depend on how closely we are able to mimic the operating principles of the olfactory system. As biologists and biochemists learn more about the olfactory receptors and biological amplification systems employed to detect extremely low odorant concentrations, we hope to apply the same principles to our artificial system.

Recently we have developed a technique for creating sensor diversity using polymer mixtures.[43] We observed that the response from a sensor made by polymerizing two monomers was not a linear combination of the sensor responses from sensors made from the pure monomers. By preparing sensors with various compositions of two monomers, we found that they contained approximately the same diversity as sensors prepared from randomly selected chemically diverse polymers. We reasoned that, by creating a large number of such incremental compositional variations, we would be able to create a wide sensor diversity unachievable using conventional polymers. We created such sensor diversity by employing a polymer gradient. As shown in Figure 14, a pinhole was positioned on the imaging fiber such that it illuminated a small circular area on the fiber surface. The distal tip of the fiber was placed into a solution of a siloxane prepolymer, PS802. By using a micropositioner, the pinhole was scanned 180° across the surface of the fiber. During scanning, a second monomer, methyl methacrylate, was added continuously to the PS802 solution. Consequently, the composition of photopolymer changed continuously as the pinhole was moved across the fiber surface. At the end of the photopolymerization the composition of the solution was 50% PS802, 50% poly(methyl methacrylate). The resulting polymer stripe contained a continually varying polymer composition. By employing an image processing program, we were able to define particular regions of interest in the polymer stripe, Figure 15. Upon exposure to organic vapors, each region of the stripe responded differently and nonlinearly, indicating that small compositional differences lead to dramatic variation in sensor response from the resulting polymers. Such variation most likely arises from heterogeneous polymerization, leading to microdomain structures within the polymer resulting in nonlinear response profiles for different regions in the polymer gradient.

Randomly Encoded Arrays

One of the limitations with all the multi-analyte sensors described above is the serial process of adding sensor elements. This process creates a practical limitation and precludes the preparation of arrays containing more than 20 sensing elements on each array surface. A recent development in our laboratory has begun to address this limitation. The ultimate goal of the sensor community is to develop sensors that are small and can measure all analytes reproducibly, sensitively, and with internal or self-calibration. We believe we have taken a step in this direction by employing randomly ordered encoded array sensors.[44] In earlier work we discovered that the cores

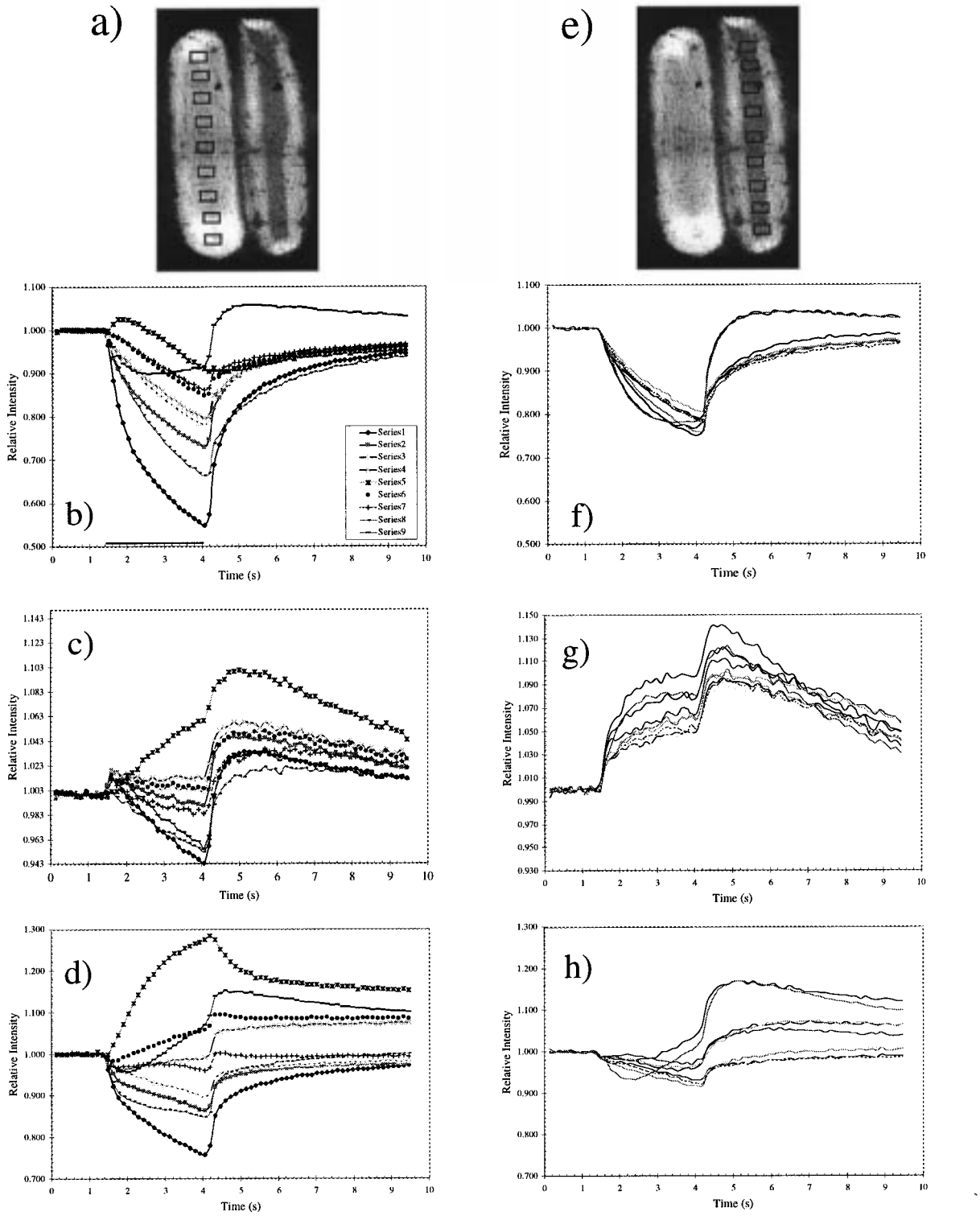

FIGURE 15. The PS802/MMA gradient sensor. Fluorescence images of the gradient (a) and PS802 control (e) polymer stripes are shown. The nine rectangular boxes represent the polymer regions monitored during the vapor pulse experiments. Responses to hexane, methanol, and benzene vapor pulses (2.6 s in length) are shown respectively in b, c, and d for the gradient stripe, and in f, g, and h for the control stripe.

in the optical arrays could be selectively etched by using a buffered HF solution.[45] We subsequently found that when a solution of latex microspheres was dripped onto the array of etched microwells, the microspheres positioned themselves into each microwell if the sizes of the microspheres and wells were matched, as shown in Figure 16. This discovery led us to a dramatically different method for preparing sensor arrays. The concept is illustrated in Figure 17. First, different populations of microspheres are prepared. Each microsphere contains a sensing chemistry and an encoding chemistry. The sensing chemistry can be any conventional analytical reagent that creates an optical signal, for example, immunoassays, enzyme-based analyses, or conventional

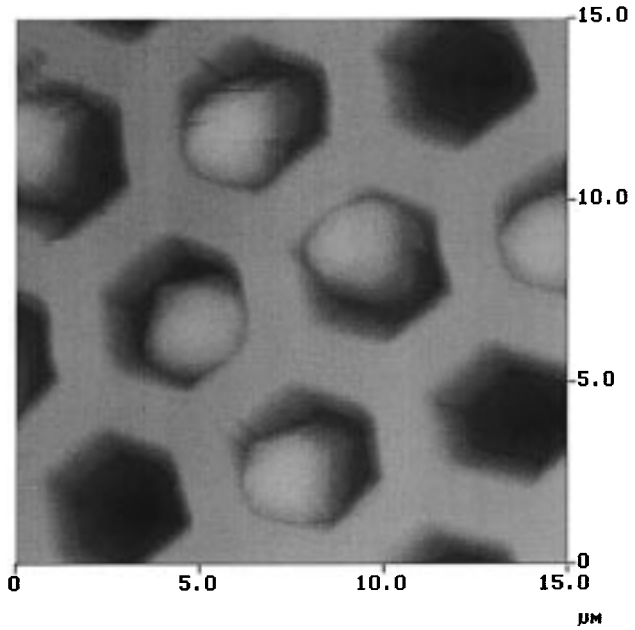

FIGURE 16. Atomic force micrograph of ~3.6-μm-diameter microwells containing a single 3.1-μm-diameter microsphere in each microwell. Three wells in field of view do not contain microspheres.

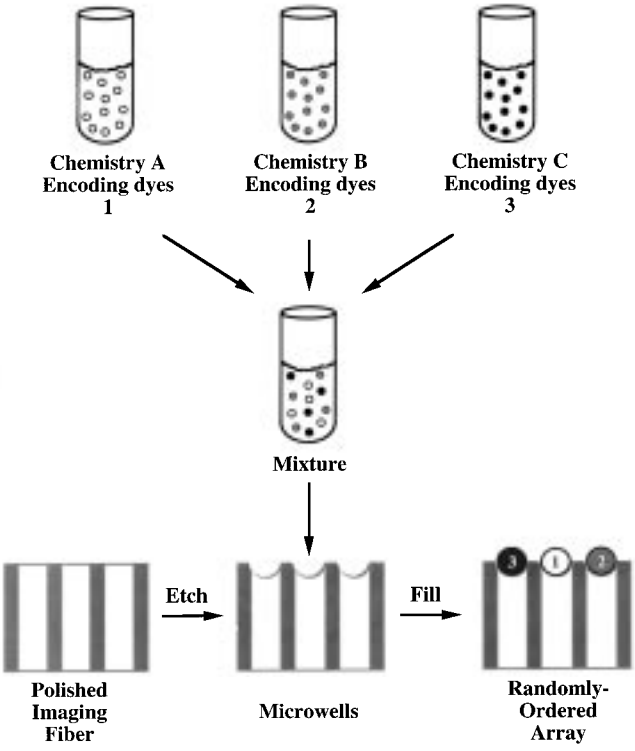

FIGURE 17. Schematic concept of a randomly ordered addressable high-density array. Separate sets of individual micrometer-sized sensors are created by covalently immobilizing indicating chemistries on the surface of microspheres. The microspheres are mixed together and randomly distributed in the wells of a chemically etched optical imaging fiber.

fluorescent indicators. This reaction chemistry is covalently attached to the beads. Each microsphere is also modified with encoding dyes to provide an optical signature identifying what analytical chemistry is contained on that particular microsphere, similar to encoding bead libraries for combinatorial synthesis.[46] A microsphere population therefore contains both a particular analytical chemistry and its signature encoding dyes. A variety of different microsphere populations are prepared. The different microspheres are then mixed to provide a population of all possible analytical chemistries of interest. Next, this mixed population is deposited in the microwell array to give a randomly distributed microsphere array. Individual arrays contain different distributions and locations of microspheres. The key is that each microsphere has an encoding signature that enables the array to be decoded. Using modern image processing software, such decoding can be accomplished in a matter of seconds. Although the sensing chemistry on each microsphere is still the essential determinant of performance, the burden of preparing sensors shifts from trying to make each sensor identical with determining what has been made after an easy fabrication step. There are many advantages with such an approach. One milliliter of microspheres contains 5.8×10^9 microspheres with nearly identical properties. Each microwell is approximately 3 μm in diameter with a volume of approximately several tens of femtoliters, thereby reducing sample volume significantly. There are multiple copies of each microsphere enabling redundant measurements from multiple sensors, thereby reducing the possibility of false positive and false negative results. Finally, as new analytical chemistries become available, the incremental effort to place an additional sensor in the array is minimal; all that is required is to attach that particular chemistry to a uniquely-encoded bead. The approach is limited by how many different types of encoded signatures can be prepared—an active area of pursuit in our laboratory.

Conclusion

The use of optical imaging fibers as an architecture for chemical sensors was first reported by us in 1991. By developing compatible polymer chemistries in association with chemically-sensitive indicators, we have demonstrated a wide variety of applications in which such sensors can make unique measurements. Multisensor arrays containing specific chemistries, arrays based on cross-reactive polymers for artificial olfactory devices, high-density encoded arrays—all provide the ability to measure multiple analytes simultaneously in small volumes via optical measurements. Furthermore, the ability to simultaneously view and measure samples has resulted in our ability to monitor the initiation of corrosion as well as neurotransmitter release over relatively large surface areas. Ultimately such an approach may be important for performing minimally invasive procedures in which simultaneous morphological and chemical information can be acquired through the chemically-modified imaging sensor. In work not discussed in this article, we have tapered the fibers to create even smaller structural features, have put microlenses on the fibers and have prepared hybrid devices containing both optical and electrochemical sensing capabilities on a single substrate.

We hope these advances and others yet to be discovered will contribute to the arsenal of sensors for chemical analysis in the future.

The author is extremely grateful to the many talented graduate students and postdoctoral co-workers who have contributed to the research described in this account. The author gratefully acknowledges the support of the National Institutes of Health, Office of Naval Research, Department of Energy, National Science Foundation, Environmental Protection Agency, and Defense Advanced Research Programs Agency for their generous support of the work.

References

(1) Tan, W.; Shi, Z.-Y.; Smith, S.; Birnbaum, D.; Kopelman, R. *Science* **1992**, *258*.
(2) Tan, W.; Shi, Z.-Y.; Kopelman, R. *Anal. Chem*. **1992**, *64*, 2985−2990.
(3) Rosenzweig, Z.; Kopelman, R. *Anal. Chem*. **1995**, *67*, 2650−2654.
(4) Bronk, K. S.; Michael, K. L.; Pantano, P.; Walt, D. R. *Anal. Chem*. **1995**, *67*, 2750−2757.
(5) Walt, D. R.; Pantano, P.; Michael, K. L.; Panova, A. *Proc. ICSOI* **1996**, *194*, 170.
(6) Michael, K. L.; Ferguson, J. A.; Healey, B. G.; Panova, A. A.; Pantano, P.; Walt, D. R. In *Polymers in Science: Theory and Practice*; Akmal, N., Usmani, A., Eds.; ACS Symposium Series 690; American Chemical Society: Washington, DC, **1998**; pp 273−289.
(7) White, J.; Kauer, J. S.; Dickinson, T. A.; Walt, D. R. *Anal. Chem*. **1996**, *68*, 2191−2202.
(8) Dickinson, T. A.; White, J.; Kauer, J. S.; Walt, D. R. *Nature* **1996**, *382*, 697−700.
(9) Pantano, P.; Walt, D. R. *Anal. Chem*. **1995**, *67*, 481A.
(10) Panova, A. A.; Pantano, P.; Walt, D. R. *Anal. Chem*. **1997**, *69*, 1635−1641.
(11) Schroeder, T. J.; Jankowski, J. A.; Senyshyn, J.; Holz, R. W.; Wightman, R. M. *J. Biol. Chem*. **1994**, *269*, 17215−17220.
(12) Garguilo, M. G.; Michael, A. C. *Anal. Chim. Acta* **1995**, *307*, 291−299.
(13) Morelis, R. M.; Coulet, P. R. *Anal. Chim. Acta* **1990**, *231*, 27−32.
(14) Tor, R.; Freeman, A. *Anal. Chem*. **1986**, *58*, 1042−1046.
(15) Montes, J. G.; Alkondon, M.; Pereira, E. F. R.; Castro, N. G.; Albuquerque, E. X. In *Methods in Neurosciences*; Narahashi, T., Ed.; Academic Press: San Diego, **1994**, Vol. 19, pp 121−147.
(16) Riklin, A.; Willner, I. *Anal. Chem*. **1995**, *67*, 4118−4126.
(17) Gray, D. B.; Bruses, J. L.; Pilar, G. R. *Neuron* **1992**, *8*, 715−724
(18) Gray, D. B.; Manthay, N.; Pilar, G. R. *Ann. N.Y. Acad. Sci*. **1991**, *635*, 408−410.
(19) Gray, D. B.; Zelany, D.; Manthay, N.; Pilar, G. R. *J. Neurosci*. **1990**, *10*, 2687−2698.
(20) Pollak, A.; Blumenfeld, H.; Wax, M.; Baughn, R. L.; Whitesides, G. M. *J. Am. Chem. Soc*. **1980**, *102*, 6324−6336.
(21) Peterson, B. A.; Weeks, J. C. J. *Comp. Neurol*. **1988**, *275*, 128−144.
(22) Trimmer, B. A.; Weeks, J. C. *J. Neurophysiol*. **1993**, *69*, 1821−1836.
(23) Healey, B. G.; Foran, S. E.; Walt, D. R. *Science* **1995**, *269*, 1078−1080.
(24) Healey, B. G.; Walt, D. R. *Anal. Chem*. **1997**, *69*, 2213−2216.
(25) Barnard, S. M.; Walt, D. R. *Nature* **1991**, *353*, 338−340
(26) Ferguson, J. A.; Healey, B. G.; Bronk, K. S.; Barnard, S. M.; Walt, D. R. *Anal. Chim. Acta* **1997**, *340*, 123−131.
(27) Xu, W.; McDonough, R. C.; Langsdorf, B.; Demas, J. N.; DeGraff, B. A. *Anal. Chem*. **1994**, *66*, 4133−4141.
(28) Uttamlal, M.; Walt, D. R. *Biotechnology* **1995**, *13*, 597.
(29) Healey, B. G.; Walt, D. R. *Anal. Chem*. **1995**, *67*, 4471−4476.
(30) Li, L.; Walt, D. R. *Anal. Chem*. **1995**, *67*, 3746−3752.
(31) Wallraff, G.; Labadie, J.; Brock, P.; DiPietro, R.; Nguyen, T.; Huynh, T.; Hinsberg, W.; McGall, G. *CHEMTECH* **1997** (Feb), *47* (2), 22−32.
(32) Schena, M.; Shalon, D.; Heller, R.; Chai, A.; Brown, P. O.; Davis, R. W. *Proc. Natl. Acad. Sci. U.S.A.* **1996**, *93*, 10614−10619.
(33) Chee, M.; Yang, R.; Hubbell, E.; Berno, A.; Huang, X. C.; Stern, D.; Winkler, J.; Lockhart, D. J.; Morris, M. S.; Fodor, S. P. A. *Science* **1996**, *274*, 610.
(34) Cronin, M. T.; Fucini, R. V.; Kim, S. M.; Masino, R. S.; Wespi, R. M.; Miyada, C. F. *Human Mutation* **1996**, *7*, 244−255.
(35) Ferguson, J. A.; Boles, T. C.; Adams, C. P.; Walt, D. R. *Nature Biotech*. **1996**, *14*, 1681−1684.
(36) Healey, B. G.; Matson, R. S.; Walt, D. R. *Anal. Biochem*. **1997**, *251*, 270−279.
(37) Halasz, N. *The Vertebrate olfactory system: chemical neural anatomy, function & development*; Akadémiai Kiadó: Budapest, 1980.
(38) Buck, L.; Axel, R. *Cell* **1991**, *65*, 175−187.
(39) Kauer, J. S. *Trends Neurosci*. **1991**, *14*, *79−85*.
(40) Lippert, Von E. *Z. Electrochem*. **1957**, *61*, 962−975.
(41) Lakowicz, J. *Principles of Fluorescence Spectroscopy*; Plenum Press: New York, 1982.
(42) Barnard, S. M.; Walt, D. R. *Environ. Sci. Technol*. **1991**, *25*, 1301−1304.
(43) Dickinson, T. A., Walt, D. R., White, J., Kaver, J. S. *Anal. Chem*. **1997**, *69*, 3413−3418.
(44) Michael, K. L.; Taylor, L. C.; Schultz, S. L.; Walt, D. R. *Anal. Chem*. **1998**, *70*, 1242−1248.
(45) Pantano, P.; Walt, D. R. *Chem. Mater*. **1996**, *8*, 2832−2835.
(46) Czarnik, A. W. *Curr. Opin. Chem. Biol*. **1997**, *1*, 60−66.

AR970069K